ACS APPLIED MATERIALS & INTERFACES

Research Article

www.acsami.org

Tumor Accumulation, Penetration, and Antitumor Response of Cisplatin-Loaded Gelatin/Poly(acrylic acid) Nanoparticles

Dan Ding,[†] Jing Wang,[†] Zhenshu Zhu,[†] Rutian Li,[‡] Wei Wu,[†] Baorui Liu,[‡] and Xiqun Jiang*,[†]

[†]Laboratory of Mesoscopic Chemistry and Department of Polymer Science & Engineering, College of Chemistry & Chemical Engineering, Nanjing University, Nanjing 210093, P. R. China

[‡]Comprehensive Cancer Center of Drum Tower Hospital, Medical School of Nanjing University & Clinical Cancer Institute, Nanjing University, Nanjing 210008, P. R. China

ABSTRACT: In this report, the cisplatin (CDDP)-loaded gelatin/poly(acrylic acid) (GEL-PAA) nanoparticles with a spherical shape and drug loading content of 24.6% were prepared. In vivo near-infrared fluorescence (NIRF) imaging and ex vivo gamma scintillation counting analyses reveal that CDDP-loaded GEL-PAA nanoparticles have prominent passive tumor-targeting ability and the nontarget nanoparticles can be readily excreted from the body. Further, it is demonstrated that the CDDP-loaded nanoparticles have the ability to penetrate the tumor after their extravasation through the leaky vessels and distribute in a distance of about 20 μm from the vessels at 24 h postinjection. The in vivo antitumor responses reveal that the nanoparticle formulation exhibits significantly superior in vivo antitumor effect than free CDDP by the comparison of tumor volume and the examinations of cell apoptosis and proliferation in tumor tissues through proliferating cell nuclear antigen (PCNA) and terminal deoxynucleotidyl-transferase-mediated nick end labeling (TUNEL) methods.

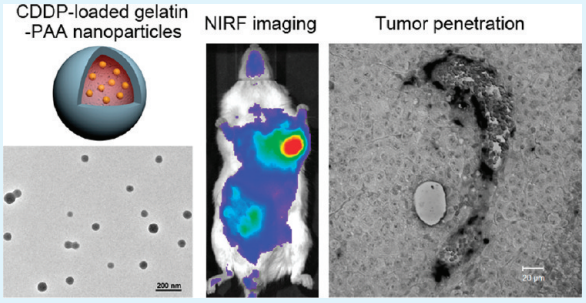

KEYWORDS: *gelatin nanoparticles, drug delivery, antitumor response, cisplatin, tumor penetration, in vivo imaging*

INTRODUCTION

The development of polymeric nanoparticles has been attracting considerable interest in recent years due to their promising applications in cancer therapy.[1−4] They are able to preferentially accumulate in tumor tissues by passive targeting through the enhanced permeability and retention (EPR) effect or active targeting by ligand−receptor interactions or highly specific interactions of antibodies, aptamers, peptides, and oligonucleotides with cell surface receptors.[5−8] The targeting ability of polymeric nanoparticles in vivo can be explored through various kinds of biomedical imaging technologies.[9−11] For instance, the noninvasive near-infrared fluorescence (NIRF) imaging technique has been demonstrated to be a very useful tool to evaluate the real-time information of the tumor targeting ability and in vivo biodistribution of fluorescence dye-labeled nanoparticles.[4,12] In addition, radiolabeled nanoparticles, on the basis of radioactive tracing, have been used to probe quantitatively their in vivo behavior.[13,14] Although many drug-encapsulated polymeric nanoparticles have exhibited greater antitumor efficacy and less toxicity than free drug in animal tests, it has also been suspected that the nanoparticles may not penetrate tumor tissue deeply to affect all of the viable cells, resulting in limited therapeutic effect and tumor regeneration.[15,16] The poor spread of common antitumor agents in tumors have been ascribed to the increased interstitial fluid pressure caused by leaky vasculature and poor lymphatic drainage of tumor, complex extracellular matrix (ECM), and their binding within the tumor.[15−18] However, most investigations have focused on the antitumor efficacy or in vivo biodistribution of the nanoparticles,[4,5,12−14] few if any studies on the penetration of polymeric nanoparticles in solid tumors in vivo have been reported, though it is critical for the effectiveness of tumor chemotherapy. So far, fluorescence labeling technique is the most frequently used method to assess nanoparticle penetration in solid tumors through investigating the distribution of fluorescently labeled nanoparticles referenced to tumor blood vessels.[19,20] However, the observation of nanoparticles in tumor tissues often suffers from the disturbance of the intense background autofluorescence of tumor tissues. Hence, the development of a more efficient strategy is highly desirable to exactly and clearly recognize the location of polymeric nanoparticles in solid tumors.

In the current work, we developed cisplatin (CDDP)-loaded gelatin/poly(acrylic acid) (GEL-PAA) nanoparticles with high drug loading content (24.6%) for systemic chemotherapy. The preparation of GEL-PAA nanoparticles, which are biocompatible and stable in aqueous solution, was reported in our previous study via the polymerization of acrylic acid monomers in the presence of gelatin in aqueous solution.[21] CDDP, which is one of the most effective antitumor agents but has severe side effects,[4] was successfully loaded into the GEL-PAA nano-

Received: January 24, 2012
Accepted: February 24, 2012
Published: February 24, 2012

particles through a ligand exchange reaction of platinum(II) from the chloride to the carboxyl group of the nanoparticles.[22] Furthermore, the abundant carboxylic groups bound by the GEL-PAA nanoparticles make it possible to enhance the drug loading content of CDDP with respect to pure gelatin nanoparticles. In this study, we report the investigations on the fate and biodistribution of CDDP-loaded GEL-PAA nanoparticles in tumor-bearing mice by conjugating NIRF probe and radioactive nuclide to GEL-PAA nanoparticles. In addition, we developed a biotinylated GEL-PAA nanoparticle complexed with CDDP to efficiently evaluate their penetration in tumor tissues using a biotin−avidin system, avoiding the interference of tumor autofluorescence. To our knowledge, this is the first case concerning the application of biotin−avidin interaction in investigating the penetration of polymeric nanoparticles in solid tumor. Finally, we also assessed the antitumor activity of CDDP-loaded GEL-PAA nanoparticles after intravenous (i.v.) injection by measuring the evolvement of tumor volumes and survival rates of tumor-bearing mice and by employing the proliferating cell nuclear antigen (PCNA) and terminal deoxynucleotidyl-transferase-mediated nick end labeling (TUNEL) assays.

EXPERIMENTAL SECTION

Materials. Cisplatin (CDDP) was kindly provided by Jiangsu Hengrui Pharmaceutical Co. Ltd. (Lianyungang, China). Type-B gelatin (225 bloomstrength), with 100−115 mmol of carboxylic acid per 100 g of protein, an isoelectric point of 4.7−5.2, and an average molecular weight of 40−50 kDa, was purchased from Sigma-Aldrich (St Louis, MO), and was refined once by dissolving it in distilled water followed by precipitating with acetone and drying in a vacuum at room temperature. Acrylic acid (AA) (Guanghua Chemical Company, Shanghai, China) was distilled under reduced pressure in nitrogen atmosphere. Potassium persulfate ($K_2S_2O_8$) was recrystallized from deionized water before use. *N*-(3-dimethylaminopropyl)-*N*′-ethyl-carbodiimide hydrochloride (EDC×HCl), 2,2′-(ethylenedioxy)bis-(ethylamine), and 1-(4,5-dimethylthiazol-2-yl)-3,5-diphenyl-formazan (MTT) were purchased from Aldrich. Near infrared probe, NIR-797-isothiocyanate, was purchased from Sigma Chemical Co. Biotin was bought from Shenggong Chemical Company (Shanghai, China). Alkaline phosphatase (AP) conjugated avidin and NBT/BCIP were bought from Merck (Germany). All other reagents were of analytical grade and used without further purification. Murine hepatic H22 cancer cell line and human gastric carcinoma cell line BGC823 were obtained from Shanghai Institute of Cell Biology (Shanghai, China). Male ICR mice (6−8 weeks, 22−26 g) were purchased from Animal Center of Drum-Tower Hospital (Nanjing, China).

Preparation of CDDP-Loaded GEL-PAA Nanoparticles. GEL-PAA nanoparticles were prepared by polymerization of AA in the presence of gelatin in aqueous medium.[21] Briefly, purified gelatin (0.8 g) was dissolved in 50 mL of AA (0.2 g) aqueous solution, and then, the polymerization of AA monomer was initiated by $K_2S_2O_8$ at 80 °C. When opalescent suspension appeared, suggesting the formation of GEL-PAA nanoparticles, the reaction was allowed to proceed for another 120 minutes at 80 °C. After removal of large aggregates by filtration, the resultant suspension was dialyzed against a buffer solution of pH 3.0 for 24 h using a 12 kDa MWCO membrane to remove residual monomers. Thereafter, a predetermined amount of 2,2′-(ethylenedioxy)-bis(ethylamine) together with EDC was used to cross-link the nanoparticles by reaction at room temperature for 12 h. The cross-linked product was then dialyzed against distilled water for 24 h. Then, a predetermined amount of CDDP was added in an aqueous suspension of GEL-PAA nanoparticles (2.1 mg/mL) with final concentration of 1 mg/mL. The resultant mixture was agitated gently at 37 °C for 2 days. After removal of the free drug following the reported procedures,[22] the CDDP-loaded GEL-PAA nanoparticles were characterized by dynamic light scattering (DLS, BI9000AT, Brookheaven Instruments Inc., USA) and transmission electron microscopy (TEM, JEOL TEM-100, Japan).

In Vitro CDDP Release. The release profile of CDDP from GEL-PAA nanoparticles in phosphate buffered saline (PBS) at 37 °C was assessed by the dialysis method as previously reported.[23] Briefly, a purified CDDP-loaded nanoparticle solution of known platinum drug concentration was placed inside a dialysis bag (MWCO, 12 000) and dialyzed against PBS (0.01 M phosphate buffer, pH 7.4, plus 0.15 M NaCl) at 37 °C. The released Pt outside of the dialysis bag was sampled at defined time periods and measured by ion coupled plasma-mass spectrometry (ICP-MS, Perkin-Elmer Corporation, USA).

In Vitro Cytotoxicity Evaluation. Cytotoxicity of CDDP-loaded GEL-PAA nanoparticles against low differential human gastric cancer cell line BGC823 was assessed by MTT assay.[24] Briefly, BGC823 cells were seeded in 96-well plates with a density around 5000 cells/well and allowed to adhere for 24 h prior to the assay. Then, the cells were exposed to a series of doses of free CDDP or CDDP-loaded nanoparticles at 37 °C. After 48 h of incubation, 50 μL of MTT indicator dye (5 mg/mL in PBS, pH 7.4) was added to each well and the cells were incubated for another 2 h at 37 °C in the dark. The medium was withdrawn, and 200 μL of acidified isopropanol (0.33 mL of HCl in 100 mL of isopropanol) was added in each well and agitated thoroughly to dissolve the formazan crystals. The solution was transferred to 96-well plates and immediately read on a microplate reader (Bio-Rad, Hercules, CA, USA.). Absorption was measured at a wavelength of 490 nm and 620 nm as a reference wavelength, and obtained values were expressed as a percentage of the control cells to which no drugs were added. All experiments were repeated three times.

Real-Time NIRF Imaging. NIR-797-isothiocyanate was used to label CDDP-loaded GEL-PAA nanoparticles. Briefly, NIR-797-isothiocyanate was dissolved in DMSO at 10 mg/mL. The suspension of CDDP-loaded nanoparticles was adjusted to pH 8.0 by sodium hydroxide solution (0.2N). Afterwards, 100 μL of the dye solution was added to 2 mL of nanoparticle solution and agitated gently at 37 °C for 12 h. Then, the labeled nanoparticles were purified by ultrafiltration (MWCO: 100 kDa) to remove unconjugated NIR-797. The amounts of the NIR-797 successfully conjugated in nanoparticles were determined from the photoluminescence spectra with reference to a calibration curve established from DMSO solutions of NIR-797-isothiocyanate.

All animal experiments were performed in compliance with guidelines set by the Animal Care Committee at Drum-Tower Hospital. H22 tumor cells ($4\text{-}6 \times 10^6$ cells per mouse) were inoculated subcutaneously to ICR mice at the left axilla. For NIRF imaging, H22 tumor-bearing mice (~35 g) were injected i.v. with the NIR-797 labeled and CDDP-loaded nanoparticles. Subsequently, the mice were anesthetized and placed on an animal plate heated to 37 °C. The time-dependent biodistribution in tumor-bearing mice was imaged using the IVIS Lumina system (Xenogen Co., Alameda, CA, USA). The NIRF at 745 nm was collected, and exposure time was set to 2 s. Scans were conducted at 0.5, 1, 2, 3, 6, 8, 10, 24, 36, and 48 h post i.v. injection.

Biodistribution Investigation. First, diethylenetriaminepenta-acetic (DTPA) dianhydride (synthesized following reported procedures[25]) was dissolved in DMSO at 20 mg/mL, 200 μL of which was added to a solution of CDDP-loaded nanoparticles (2 mL; pH = 8.0). Then, the mixture was stirred at room temperature overnight. Afterwards, the obtained product was purified by ultrafiltration (MWCO: 100 kDa) to remove the excess of DTPA dianhydride and its hydrolysis product. The radiolabelling of nanoparticles was based on a method as previously described.[13] In brief, stannous chloride and $^{99m}TcO_4^-$ were added to a solution of DTPA modified and CDDP-loaded nanoparticles in PBS (0.1 M, pH 7.4). The resulting mixture was stirred for 20 min at room temperature. Thereafter, the ^{99m}Tc labeled and CDDP-loaded nanoparticles were obtained by ultrafiltration (MWCO: 100 kDa). The content of ^{99m}Tc labeled in nanoparticles was measured by a NaI(T1) scintillor.

For the biodistribution studies, H22 tumor-bearing mice were injected i.v. with 0.3 mL of a saline solution of ^{99m}Tc labeled and CDDP-loaded nanoparticles at the dosage of 6 mg/kg CDDP equiv

containing 300 μCi of ^{99m}Tc. Then, the animals were sacrificed at 1, 2, 4, 6, 12, and 22 h postadministration with 5 mice for each time point (with the exception of 4 mice for 12 h). Subsequently, the tissues of each mouse including the heart, liver, spleen, kidney, lung, stomach (emptied), intestine (emptied), femur, muscle (thigh), tumor, and brain were excised, and blood was collected. The obtained blood and tissues were put into preweighed vials and counted for ^{99m}Tc activity by a γ-counter. An identical sample to that injected was also counted at each time point as a reference to eliminate the interference of the physical decay of radioactivity. The results were defined as the percentage of injected dose per gram of wet tissues (% ID/g).

Penetration in Tumor. For labeling of nanoparticles with biotin, a solution of biotin (100 mg) in 5 mL of anhydrous DMSO was activated with EDC×HCl (82.4 mg) and NHS (51.8 mg) under nitrogen for 1 h, subsequently 200 μL of which was added to a solution of CDDP-loaded nanoparticles (2 mL; pH = 7.0). The resulting mixture was stirred at room temperature for 48 h. Thereafter, the product was purified by dialysis against deionized water using a dialysis membrane bag (12 kDa cutoff) to remove unconjugated biotin. The biotin concentration in dialysis fluid was subsequently determined by high performance liquid chromatography (HPLC, Shimadzu LC-ESI spectrometer).

For penetration studies, H22 tumor-bearing mice were injected i.v. with biotinylated CDDP-loaded nanoparticles. Then, the mice were sacrificed at 4 and 24 h postadministration, respectively, with 4 mice for each time point, and tumors were dissected and fixed in 10% neutral buffered formalin as well as placed into paraffin and sectioned (4 μm). Then, the tumor slices were stained by AP conjugated avidin (50 μL per slice) to react with biotin in the nanoparticles. Then, 100 μL of NBT/BCIP was added to the tumor slice and incubated for 5 min at room temperature in dark. All tumor slices were imaged by the optical channel of Zeiss LSM 710 confocal microscope (Germany).

In Vivo Antitumor Efficacy. The tumor models were established by inoculating subcutaneously H22 tumor cells ($4-6 \times 10^6$ cells per mouse) to ICR mice at the left axilla as mentioned above. When the tumor volume reached about 100 mm^3 (~6 days after tumor inoculation), the mice were selected and this day was designated as Day 0. On day 0, the mice were randomly divided into 4 groups, and each group was composed of 8 mice. Then, the mice were administered via tail vein with neat saline, empty nanoparticles, free CDDP, or CDDP-loaded GEL-PAA nanoparticles. Free CDDP and CDDP-loaded nanoparticles were given once every 5 day at 6 mg/kg on a CDDP basis, respectively. The tumor volumes were measured every other day using calipers for 17 days. The tumor volume was calculated as $D \times d^2/2$, where D was the longest and d the shortest diameter. Otherwise, the clinical stations and survival rates of mice were also monitored throughout the study.

The tumor growth inhibition (TGI) was calculated by the following equation:

$$\mathrm{TGI} = (1 - V \text{ of tested group}/V \text{ of saline group}) \times 100\%$$

where V is the average tumor volume.

Determination of Cell Apoptosis and Proliferation. Tumors from mice that received different treatments were excised at day 7 (3 mice per group). The tumors were dissected and fixed in 10% neutral buffered formalin. Then, the tissues were processed routinely into paraffin, sectioned at a thickness of 4 μm. Proliferating cells were detected using an antibody against PCNA and visualized by incubation with 3,3′-diaminobenzidine tetrahydrochloride (Aldrich) for 2 min. After being rinsed with distilled water, the sections were counterstained with hematoxylin. TUNEL staining was performed following manufacturer's instruction of In Situ Cell Death Detection Kit (Roche, Indianapolis, IN) to detect apoptotic cells. For quantification of PCNA and TUNEL expression, the number of positive cells was counted in 6 random high power fields (×200 magnification) and divided by the total number of cells for each tumor slice.

Statistical Analysis. Quantitative data were expressed as mean ± SD. Statistical comparisons were made by one-way ANOVA analysis and Student's t-test. P value < 0.05 was considered statistically significant.

RESULTS AND DISCUSSION

Preparation of GEL-PAA Nanoparticles for CDDP Delivery and Imaging. In a previous work,[21] we have demonstrated that biocompatible GEL-PAA nanoparticles could be synthesized using a polymer−monomer pair method,[26,27] followed by selective cross-linking of carboxylic groups in the nanoparticles via 2,2′-(ethylenedioxy)bis-(ethylamine). It was also found that the cross-linked GEL-PAA nanoparticles were stabilized by an outer layer of GEL with ionized carboxylic groups at pH 7.4.[21] More importantly, the abundant functional groups in the nanoparticles, such as amino and carboxyl groups, allow subsequent drug encapsulation and chemical modification. Hence, CDDP was successfully loaded into GEL-PAA nanoparticles by a ligand exchange reaction of platinum(II) from the chloride to the carboxyl group of the nanoparticles.[22] The drug loading content and encapsulation efficiency is 24.6±1.2% and 68.7±4.6%, respectively, with the initial feed amount of [CDDP]/[COOH of nanoparticles] = 1:2. The high drug payload is attributed to the PAA chains in the nanoparticles providing a large amount of carboxylic groups, which also indicates that PAA component remains in the nanoparticles after cross-linking and dialysis. The dynamic light scattering (DLS) result reveals that the mean size of the obtained CDDP-loaded GEL-PAA nanoparticles is ~90 nm. Moreover, transmission electron microscope (TEM) was performed to investigate the morphology of both the nanoparticles with and without CDDP, as shown in Figure 1A. The CDDP-loaded nanoparticles have a spherical outline with an average size of about 60 nm, which is smaller than the DLS result due to their shrinkage in dry state. In addition, the CDDP-loaded nanoparticles are smaller in size than the nanoparticles without CDDP loading (about 100 nm), due to the cross-linking of COOH groups of nanoparticles by Pt complex formation.[28]

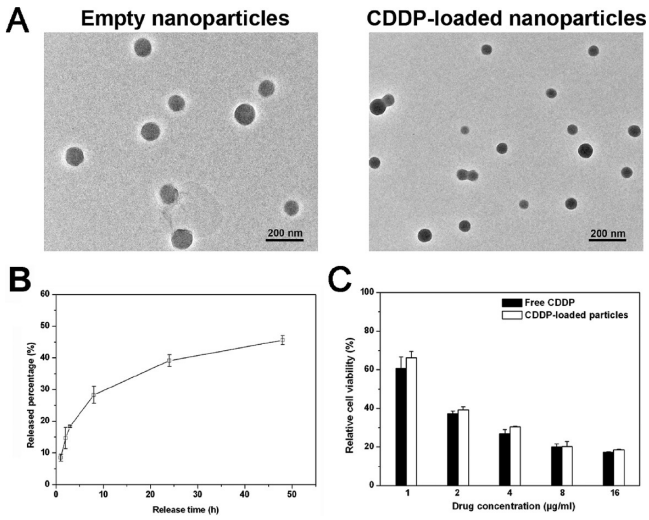

Figure 1. (A) The morphology of empty and CDDP-loaded GEL-PAA nanoparticles measured by TEM. (B) In vitro release profile of CDDP from GEL-PAA nanoparticles in PBS at 37 °C. (C) In vitro cytotoxicity of free CDDP and CDDP-loaded GEL-PAA nanoparticles against BGC823 cells.

Figure 1B shows the CDDP release profile of CDDP-loaded GEL-PAA nanoparticles in phosphate buffered saline (PBS) at 37 °C. Since the media contains chloride ions, the drug-loaded nanoparticles can release CDDP by an exchange reaction

between the chloride ions and carboxylic groups of the nanoparticles.[29] As depicted in Figure 1B, the release of CDDP is in a sustained manner from the nanoparticles after an initial burst of drug release in the first 8 h. In addition, in vitro cytotoxicity test of CDDP-loaded nanoparticles using cultured human gastric cancer BGC823 cells was conducted (Figure 1C). It can be seen that CDDP-loaded nanoparticles exhibit similar cytotoxic activity to free CDDP at all tested concentrations after 48 h incubation. The similar cytotoxicity may result from the gelatin-based nanoparticles that can efficiently internalize in the cell and mainly localize in the cytoplasm.[21]

We next labeled the CDDP-loaded nanoparticles with different functional molecules via the amino groups of GEL-PAA nanoparticles. As shown in Figure 2, the CDDP-loaded

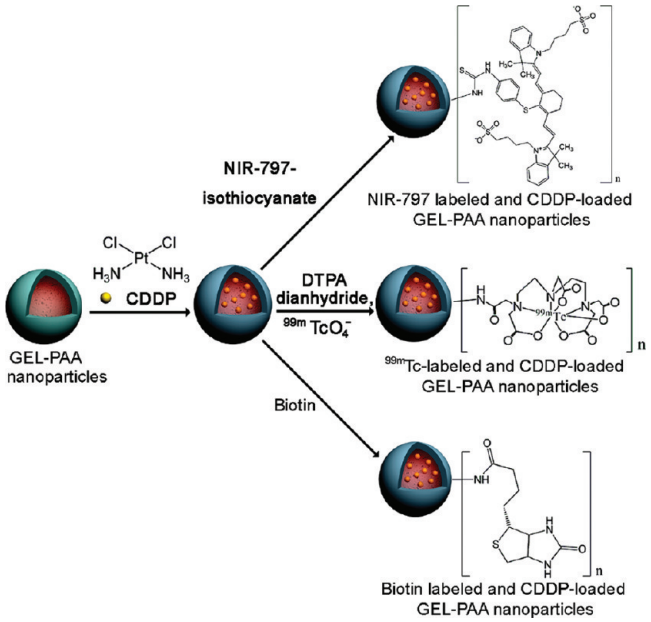

Figure 2. Scheme of the preparation and labeling of CDDP-loaded GEL-PAA nanoparticles.

nanoparticles were labeled with NIR-797 for NIRF imaging in vivo or biotin for monitoring the permeation of nanoparticles in tumors. Besides, after reacting with diethylenetriaminepentaacetic (DTPA) dianhydride via the amino groups of nanoparticles, the CDDP-loaded nanoparticles were also labeled with radioactive nuclide technetlum-99m for gamma scintillation counting analysis.

In Vivo Imaging of CDDP-Loaded GEL-PAA Nanoparticles. To investigate the fate of CDDP-loaded GEL-PAA nanoparticles in a living system, the noninvasive and real-time near-infrared fluorescence (NIRF) imaging technique was used to visualize the tissue distribution of the nanoparticles in vivo. The CDDP-loaded GEL-PAA nanoparticles were labeled with a NIRF dye, NIR-797, and then injected into subcutaneous hepatic H22 tumor-bearing mice via the tail vein. The content of NIR-797 in nanoparticles is measured to be 54.2 μmol/g nanoparticles. Figure 3A displays the time-dependent tumor accumulation and excretion profile of NIR-797 labeled and CDDP-loaded nanoparticles in a living body. The different fluorescence intensities are represented by different colors as shown in the color histogram. It can be clearly seen from the images that intense NIRF signals are concentrated on the abdomen of the mouse in the first 3 h, which show and move along the intestinal track and then decrease over time. Generally, nanoparticles have a tendency to undergo reticuloendothelial system (RES) uptake owing to their relatively large sizes, especially in the liver.[30,31] Thus, it can be suggested that the CDDP-loaded nanoparticles of liver uptake can be excreted via biliary pathway; that is, from liver to bile duct, intestine, and finally to feces.[32] The more striking feature is that NIRF intensity in tumor tissue became stronger and stronger as the time elapsed. Quantitative data of fluorescence intensity for tumor were acquired by detecting total photon counts at tumor site. As shown in Figure 3B, the fluorescence intensity at the tumor site increases significantly in the initial 24 h postadministration, indicated by a 4.5-fold increase in total photon counts at the tumor site at 24 h compared with that at 0.5 h ($(7.7\pm0.006) \times 10^6$ versus $(1.7 \pm 0.001) \times 10^6$). Encouragingly, it seems that the nanoparticles cannot be rapidly cleared from tumor tissue, although a slight decrease in fluorescence intensity for the tumor from 24 to 48 h is observed. The remarkable tumor targeting ability of CDDP-loaded GEL-PAA nanoparticles could result from the EPR effect. Besides, a portion of the nanoparticles may have the ability to escape from the RES uptake, leading to a long blood circulation time due to their relatively smaller size. These results suggest that CDDP-loaded GEL-PAA nanoparticles can significantly passively target and accumulate in the tumor tissues, exhibiting prominent EPR effect. In the meantime, the nanoparticles that are not accumulated into tumors are able to be readily cleared from liver and other tissues, implying the minimal side effects of the drug.

Biodistribution of CDDP-Loaded GEL-PAA Nanoparticles. The radioactive tracing has been demonstrated to be a straightforward and highly sensitive technique so as to quantitatively investigate the in vivo behavior of nanomaterials recently.[13] Thus, to quantitatively estimate the biodistribution and tumor targeting ability of CDDP-loaded GEL-PAA nanoparticles in mice bearing subcutaneous H22 tumors, we labeled nanoparticles with radioactive nuclide technetlum-99m (^{99m}Tc; $T_{1/2}$ = 6.02 h, E_γ = 141 keV), which shows the characteristics of stable labeling and proper radiant energy.[13] The content of ^{99m}Tc labeled in nanoparticles is determined to be ~400 mCi/g nanoparticles. Then, tumor-bearing mice were intravenously administered with the radiolabeled nanoparticles, followed by organ excision and gamma scintillation counting analysis of their distribution in various organs and blood at multiple time points. As displayed in Figure 4, the ^{99m}Tc-labeled nanoparticles are rapidly distributed throughout most of the tissues via blood circulation. Blood sampling reveals that injected dose (ID)% per gram of blood is sharply decreased over monitoring periods of up to 22 h. However, there is still ~0.75% ID/g remaining in the blood of mice at 22 h postinjection (p.i.). The tissue distribution data reveal relatively low uptake of nanoparticles in the brain, muscle (thigh), and heart, while relatively high and moderate uptake in the tumor, liver, spleen, kidney, femur, stomach, intestine, and lung. It is known that proteins in the plasma can bind to nanoparticles after i.v. administration, termed "opsonization", for recognition by macrophages residing in the RES or mononuclear phagocyte system (MPS) tissues, including liver, spleen, and bone marrow.[33,34] Therefore, the high nanoparticle accumulation in liver, spleen, and femur is a result of RES and MPS uptake. For tumor tissue, the maximum accumulation of GEL-PAA nanoparticles occurs at 22 h p.i., which is ~6.2% ID/g,

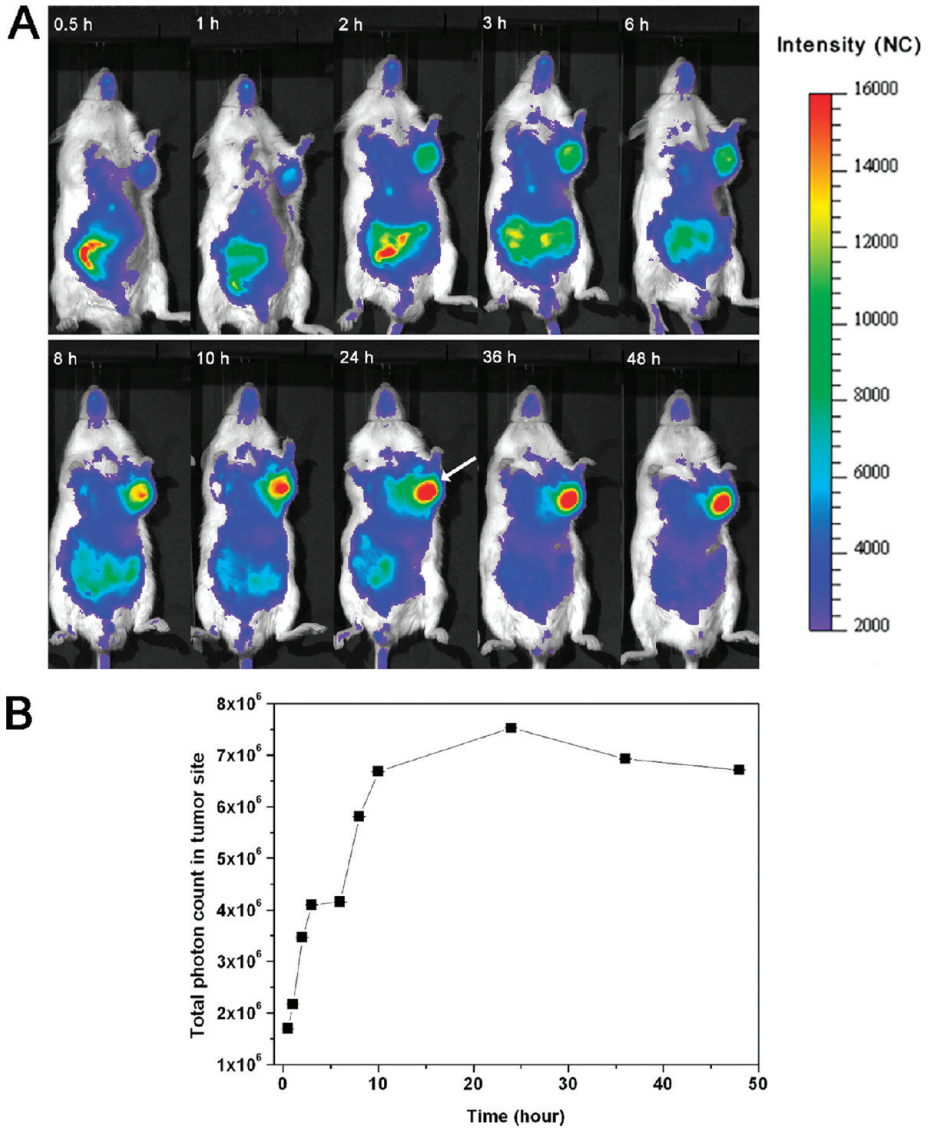

Figure 3. (A) In vivo NIRF images of H22 tumor-bearing mice after i.v. injection of NIR-797 labeled and CDDP-loaded GEL-PAA nanoparticles. The arrow indicates the location of tumor tissue. (B) The fluorescence intensity for the region of interest (tumor) was recorded as total photon counts per tumor.

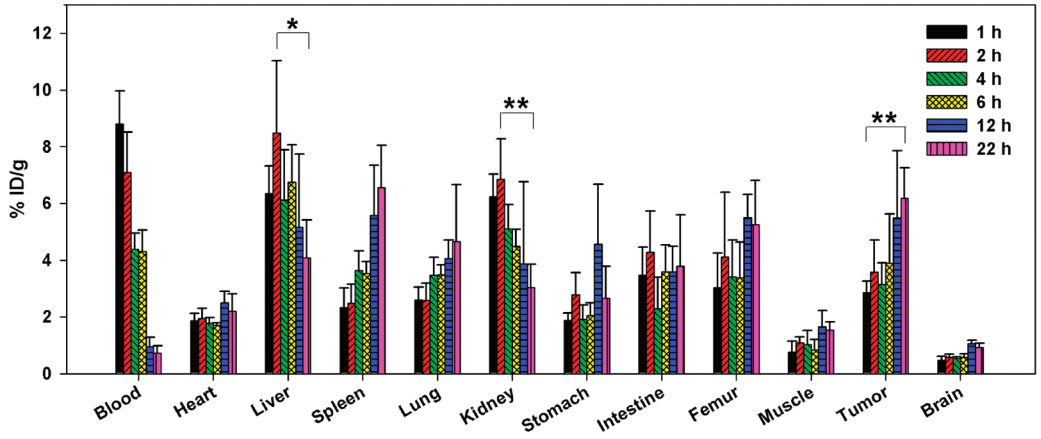

Figure 4. Biodistribution of ^{99m}Tc-labeled and CDDP-loaded GEL-PAA nanoparticles in different organs of H22 tumor-bearing mice at various time points after i.v. injection. The values were presented as the percentage of ID per gram of collected organs (5 mice per time point with the exception of 4 mice for 12 h). * and ** represent statistical significance ($P < 0.05$ and $P < 0.01$, respectively) between the values at 2 and 22 h p.i..

dx.doi.org/10.1021/am300138z | ACS Appl. Mater. Interfaces 2012, 4, 1838−1846

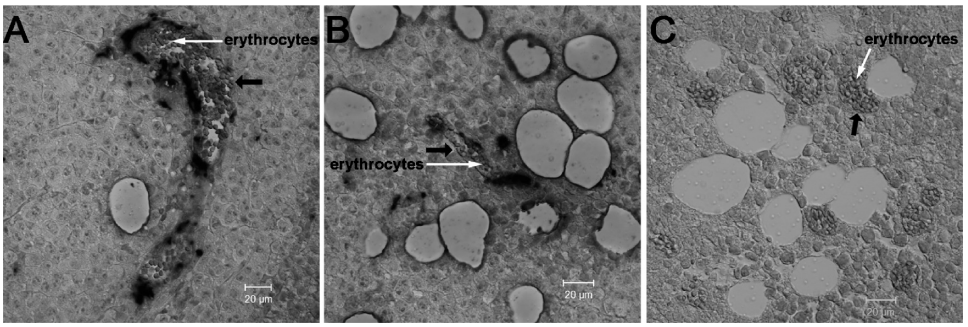

Figure 5. Penetration of biotinylated CDDP-loaded GEL-PAA nanoparticles in H22 tumors. Typical optical images of tumor slices taken from H22 tumor-bearing mice at 4 h (A) and 24 h (B) after i.v. injection of nanoparticles. (C) Representative image of H22 tumor slices from mice treated with saline. The typical blood vessels are indicated with black arrows.

elevating significantly ~2.2-fold over that at 1 h p.i. ($P < 0.01$). This result is in good accordance with the tumor observations in in vivo NIRF imaging, demonstrating the prominent EPR effect of our nanoparticles once more. It is also noteworthy that the maximal activity in liver and kidney both occurs at 2 h p.i., followed by significant elimination as time elapsed (4.08 ± 1.33 % ID/g at 22 h p.i. versus 8.48 ± 2.54 % ID/g at 2 h p.i., $P < 0.05$ for liver; 3.03 ± 0.83 % ID/g at 22 h p.i. versus 6.86 ± 1.42 % ID/g at 2 h p.i., $P < 0.01$ for kidney). It can be speculated that the nanoparticles can be excreted from the body not only through the biliary pathway from the liver as discussed earlier but also via the renal route. Moreover, relatively high uptake of nanoparticles in intestine within 24 h p.i. also suggests that the excretion of nanoparticles is through the biliary pathway. Hence, it is reasonable to say that the GEL-PAA nanoparticle drug delivery is promising for high treatment efficacy and minimum adverse effects for cancer therapy.

Penetration of CDDP-Loaded GEL-PAA Nanoparticles in Tumor. It is well known that the accumulation of drug-loaded nanoparticles in tumor tissues by EPR effect is important. Nevertheless, the subsequent penetration in tumors for drug-loaded nanoparticles is more significant to achieve effective chemotherapy index.[15,35] Thus, it is crucial to directly observe the distribution and penetration of CDDP-loaded GEL-PAA nanoparticles through the tumor. To achieve better contrast or staining effect in tumor, we have developed a new nanoparticle-labeled approach to identify the nanoparticles in tumor. The CDDP-loaded nanoparticles were first labeled by biotin with the content of biotin in nanoparticles of 1.02 mmol/g nanoparticles, and then, we injected the biotinylated nanoparticles into subcutaneous H22 tumor-bearing mice via the tail vein; the tumors were resected from the mice at 4 and 24 h p.i., respectively. Then, the tumor slices were stained by alkaline phosphatase (AP) conjugated avidin to react with biotin in the nanoparticles due to the specific binding affinity between biotin and avidin.[36] The reaction of AP with NBT/BCIP substrate yields an intense, insoluble black-purple precipitate,[37] which made the nanoparticles bring a distinguishable color in the tumor slice. As shown in Figure 5, the blood flow in the tumor vessels can be clearly observed as indicated by a large fraction of erythrocytes. The black spots are clusters of extravasated GEL-PAA nanoparticles. It can be seen from Figure 5A that most nanoparticles seem to be located in or around the blood vessels at 4 h p.i., suggesting that a number of nanoparticles in the blood can passively extravasate through the leaky vessels by EPR effect. Furthermore, it is noteworthy that more nanoparticle extravasation is observed at 24 h p.i.. As shown in Figure 5B, although some black spots are still distributed in the vascular lumen, most are found outside of the tumor vasculature and within a distance of about 20 μm from the vessels, demonstrating that the CDDP-loaded GEL-PAA nanoparticles have the ability to penetrate further away from the blood vessels and affect more viable cancer cells as the time elapsed. As the control, no black spots can be seen in the saline-treated tumors, as displayed in Figure 5C.

It is also known that the penetration of nanoparticles through tumor mass is impaired by some physiological barriers created by abnormal tumor physiology, especially the abnormal ECM and high interstitial fluid pressure.[15−18] Thus, the spread of both nanoparticle itself and drug delivered by nanoparticles in tumor mass is seriously confronted by these barriers, and they cannot affect the cells distant from the tumor vessels, which may be one of the reasons why most nanoparticle treatments cannot eradicate the tumors completely. In our case, the deeper penetration of CDDP-loaded GEL-PAA nanoparticles in tumors at 24 h p.i. should effectively improve the distribution of the delivered drugs in whole tumor tissue, which may signify more superior antitumor efficacy. As the ECM is mainly composed of collagen,[16] the good affinity between gelatin nanoparticles and the ECM may favor the improved penetration.

In Vivo Antitumor Efficacy of CDDP-Loaded GEL-PAA Nanoparticles. We next evaluated the antitumor efficacy of CDDP-loaded GEL-PAA nanoparticles compared with free CDDP in the mice bearing subcutaneous inoculated H22 tumors. There are two reasons that make us choose H22 tumor as a model. Firstly, liver cancer (hepatocellular carcinoma) is the third most common cancer in the world and a major threat to public health in Asia. Secondly, H22 transplanted solid tumor model is a fast-growing tumor model which will fluidify and quickly accrete if antitumor agents are not efficiently delivered to the tumor.[38] The treatments were done by injecting free CDDP and CDDP-loaded GEL-PAA nanoparticles (at the same CDDP dose of 6 mg/kg for two formulations, once every 5 days) i.v. into tumor-bearing mice. In two control groups, the mice were i.v. administered either saline or empty GEL-PAA nanoparticles. All of the mice were observed daily for clinical symptoms, and the tumor volume was measured every other day. Figure 6A depicts the growth curves of H22 tumors in mice receiving different treatments during therapy. It is shown that the tumor sizes in saline group and empty nanoparticles group display a rapid and time-related increase, which means that these two treatments have no measurable efficacy on impeding tumor growth. The mean

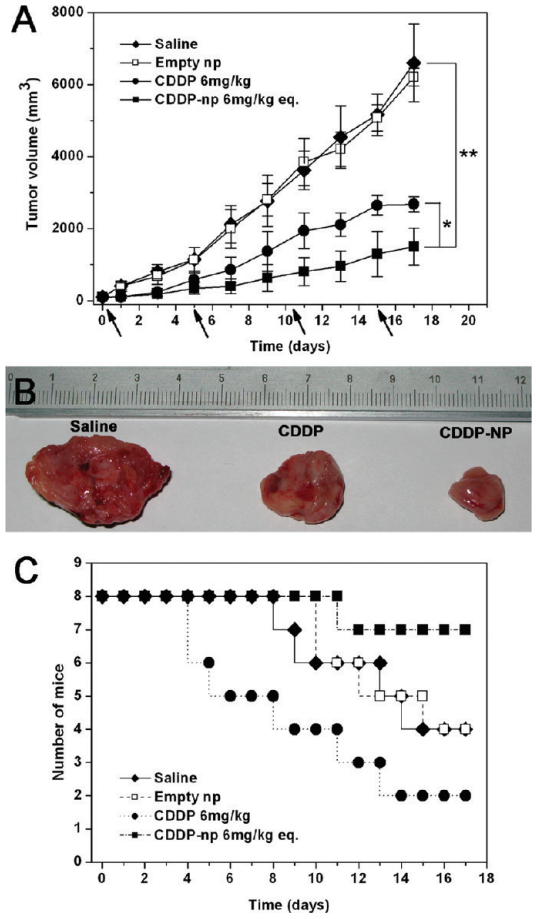

Figure 6. (A) In vivo tumor growth curves of H22 tumor-bearing mice that received different treatments indicated. The same CDDP dose (6 mg/kg) was injected for free CDDP and CDDP-loaded GEL-PAA nanoparticles on days 0, 5, 10, and 15, marked by arrows. Data are presented as mean ± SD (n = 8). * P < 0.05 and ** P < 0.01. (B) Typical images of excised tumors form mice on the 17th day after treatments with saline, free CDDP, and CDDP-loaded nanoparticles. (C) Kaplan-Meier curves showing survival of tumor-bearing mice treated with different protocols indicated.

tumor sizes of mice in saline and empty nanoparticles groups were 6602.7 ± 1077 and 6211.5 ± 243.5 mm^3, respectively, on day 17. On the contrary, the mice that received CDDP-loaded nanoparticles (6 mg/kg eq.) show the smallest tumor volumes and slowest tumor growth rates, resulting in a mean tumor volume of only 1505.9 ± 513.5 mm^3 and tumor growth inhibition (TGI) of 77.2% on the 17th day. The difference of tumor volume between the group of CDDP-loaded nanoparticles and saline is highly significant (P < 0.01). Encouragingly, it is noted that CDDP-loaded nanoparticles inhibit tumor growth much more efficiently than free CDDP formulation at the same CDDP dose (P < 0.05), although free CDDP group exhibits some degree of antitumor efficacy, leading to a mean tumor volume of 2680.5 ± 211 mm^3 on day 17 and a TGI of 59.4%. Moreover, as seen in Figure 6B, a photo of representative tumors taken from mice receiving various treatments can also illustrate the distinct tumor suppression effects as visual evidence.

The superior in vivo therapeutic efficacy of CDDP-loaded nanoparticles over that of free CDDP should be ascribed to the existence of GEL-PAA nanoparticles. Since antitumor activity of CDDP relies on its dose and exposure time in tumor site,[39] the remarkably high accumulation and retention of nanoparticles in tumor by EPR effect, as suggested by in vivo NIRF imaging and the scintillation counting results for tumor, can result in high drug content and long exposure time of CDDP on the target. In addition, the penetration of the nanoparticles into tumors also makes contribution to the enhancement of drug therapy index.

The antitumor efficacies of each treatment group were also demonstrated by evaluating the survival time of tumor-bearing mice. As shown in Figure 6C, half of the mice in the saline group and the empty nanoparticles group died during the 17-day study, due to the the fast growth of H22 tumor in ICR mice.[38] Notably, only 2 of the 8 mice in the free CDDP cohort survived 17 days, which should be attributed to the well documented severe side effects of CDDP in vivo. This observation is consistent with some reports with the rapid and high death rates of mice after i.v. injection of free CDDP.[4] However, it was found that 7 of 8 mice treated with CDDP-loaded nanoparticles could survive the 17-day study duration, greatly prolonging the lifespan of tumor-bearing mice compared with that for the free CDDP cohort. In addition, the mice treated with CDDP-loaded nanoparticles presented an active state, unlike those receiving free CDDP with decreased activity and anorexia. This result suggests the reduced side effects of nanoparticle formulation, which should result from the GEL-PAA nanoparticles that significantly change the biodistribution of the loaded drug. Besides, the results that the nontargeted nanoparticles can be readily excreted from the mice as demonstrated earlier may be also responsible for the obvious lack of toxicity in CDDP-loaded nanoparticles group.

To verify the tumor suppression mechanism, TUNEL staining was conducted to examine the apoptosis level in the tumors[20] from different cohorts (Figure 7A). The percentage of TUNEL-positive cells is significantly higher in tumors from mice that received CDDP-loaded nanoparticles compared with that in tumors of the free CDDP cohort (48.8 ± 22.2 % versus 31.3 ± 14.6 %, P<0.05) and other groups (Figure 7C). We also performed the PCNA assay to stain proliferation active cells[40] in the tumors from mice treated with various treatments. As shown in Figure 7B, as expected, a high proliferation level is observed in saline-treated and empty naoparticles-treated tumors. In contrast, the percentage of PCNA-positive tumor cells greatly decreases in the drug-loaded nanoparticles group and is significantly lower than that for the free CDDP cohort (38.8 ± 13.0 % versus 56.4 ± 25.4 %, P < 0.05; Figure 7C). Hence, both TUNEL staining and PCNA staining results further corroborate the superior antitumor efficacy of CDDP-loaded GEL-PAA nanoparticles than the other formulations.

CONCLUSIONS

In this paper, CDDP was loaded into the GEL-PAA nanoparticles through the interaction between the platinum of CDDP and the carboxylic group of the nanoparticles. The high drug loading content (24.6±1.2%) is achieved due to the large amount of carboxylic groups in the nanoparticles. The obtained nanoparticles show a spherical structure with a mean diameter of about 90 nm measured by DLS, release the CDDP in a sustained manner, and exhibit similar in vitro cytotoxic activity to free CDDP after a 48 h co-incubation with BGC823 cells. In vivo NIRF imaging and gamma scintillation counting analyses reveal that CDDP-loaded GEL-PAA nanoparticles have prominent passive tumor targeting ability and the nontarget nanoparticles can be readily excreted from the

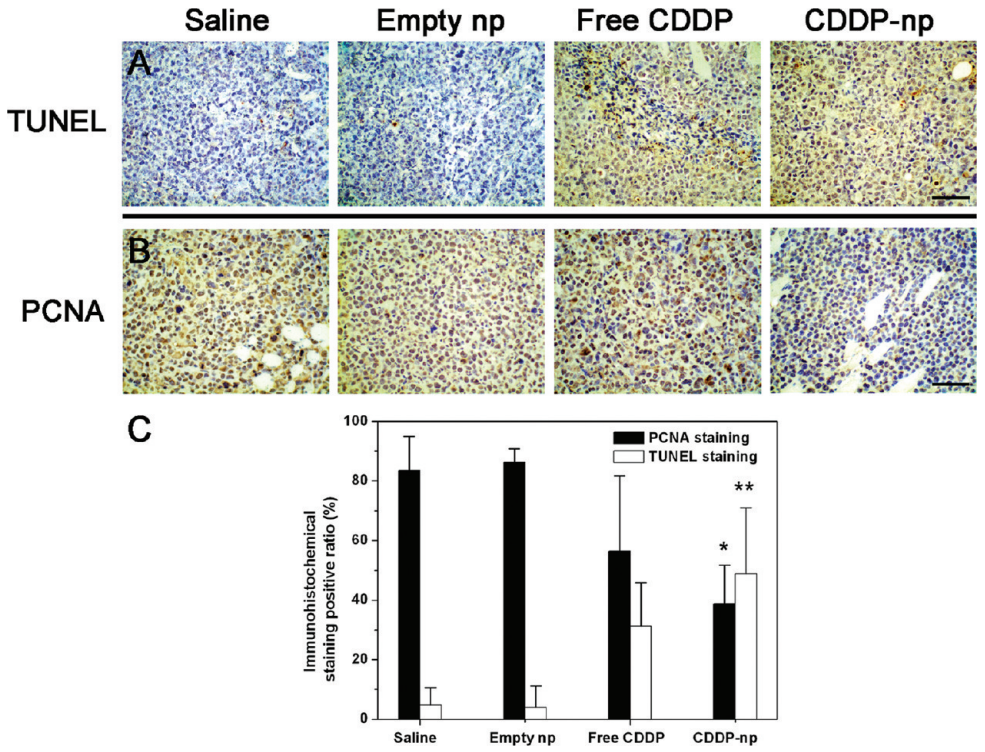

Figure 7. Immunohistochemical staining for H22 tumor from mice that received different treatments indicated for TUNEL (apoptosis assay, A) and PCNA (proliferation assay, B) staining at day 7 after therapy. (C) Quantification of TUNEL staining- and PCNA staining-positive cells in H22 tumors from mice in various groups. Data are presented as mean ± SD (n = 3, 6 random microscope fields for each tumor slice). * and ** represent $P < 0.05$ versus the free CDDP group for PCNA and TUNEL staining, respectively.

body. The penetration studies of the nanoparticles in tumor tissues demonstrate that the CDDP-loaded nanoparticles have the ability to penetrate the tumor after their extravasation through the leaky vessels and distribute in a distance of about 20 μm from the vessels at 24 h p.i.. In addition, it is also found that the CDDP-loaded GEL-PAA nanoparticles show higher antitumor efficacy and lower toxicity than free CDDP, as shown by changes in tumor volumes, survival rates, immunohistological TUNEL, and PCNA data. Hence, it is reasonable to say that GEL-PAA nanoparticles have great application potential as a carrier for platinum family drugs.

AUTHOR INFORMATION

Corresponding Author

*E-mail: jiangx@nju.edu.cn.

Notes

The authors declare no competing financial interest.

ACKNOWLEDGMENTS

This study was supported by the Natural Science Foundation of China (51033002 and 20874042).

REFERENCES

(1) Gu, F.; Zhang, L. F.; Teply, B. A.; Mann, N.; Wang, A.; Radovic-Moreno, A. F.; Langer, R.; Farokhzad, O. C. *Proc. Natl. Acad. Sci. U.S.A.* **2008**, *105*, 2586−2591.
(2) Farrell, D.; Alper, J.; Ptak, K.; Panaro, N. J.; Grodzinski, P.; Barker, A. D. *ACS Nano* **2010**, *4*, 589−594.
(3) Gref, R.; Minamitake, Y.; Peracchia, M. T.; Trubetskoy, V.; Torchilin, V.; Langer, R. *Science* **1994**, *263*, 1600−1603.
(4) Kim, J. H.; Kim, Y. S.; Park, K.; Lee, S.; Nam, H. Y.; Min, K. H.; Jo, H. G.; Park, J. H.; Choi, K.; Jeong, S. Y.; Park, R. W.; Kim, I. S.; Kim, K.; Kwon, I. C. *J. Controlled Release* **2008**, *127*, 41−49.
(5) van Vlerken, L. E.; Duan, Z.; Little, S. R.; Seiden, M. V.; Amiji, M. M. *Mol. Pharmaceutics* **2008**, *5*, 516−526.
(6) Farokhzad, O. C.; Langer, R. *ACS Nano* **2009**, *3*, 16−20.
(7) Petros, R. A.; DeSimone, J. M. *Nat. Rev. Drug Discovery* **2010**, *9*, 615−627.
(8) Koo, H.; Huh, M. S.; Sun, I. C.; Yuk, S. H.; Choi, K.; Kim, K.; Kwon, I. C. *Acc. Chem. Res.* **2011**, *44*, 1018−1028.
(9) Tsai, H. C.; Chang, W. H.; Lo, C. L.; Tsai, C. H.; Chang, C. H.; Ou, T. W.; Yen, T. C.; Hsiue, G. H. *Biomaterials* **2010**, *31*, 2293−2301.
(10) Xie, J.; Chen, K.; Huang, J.; Lee, S.; Wang, J. H.; Gao, J. H.; Li, X. G.; Chen, X. Y. *Biomaterials* **2010**, *31*, 3016−3022.
(11) Lee, J. E.; Lee, N.; Kim, H.; Kim, J.; Choi, S. H.; Kim, J. H.; Kim, T.; Song, I. C.; Park, S. P.; Moon, W. K.; Hyeon, T. *J. Am. Chem. Soc.* **2010**, *132*, 552−557.
(12) Kim, J. H.; Kim, Y. S.; Park, K.; Kang, E.; Lee, S.; Nam, H. Y.; Kim, K.; Park, J. H.; Chi, D. Y.; Park, R. W.; Kim, I. S.; Choi, K.; Kwon, I. C. *Biomaterials* **2008**, *29*, 1920−1930.
(13) Wu, W.; Li, R. T.; Bian, X. C.; Zhu, Z. S.; Ding, D.; Li, X. L.; Jia, Z. J.; Jiang, X. Q.; Hu, Y. Q. *ACS Nano* **2009**, *3*, 2740−2750.
(14) Borgman, M. P.; Coleman, T.; Jolhatkar, R. B.; Geyser-Stoops, S.; Line, B. R.; Ghandehari, H. *J. Controlled Release* **2008**, *132*, 193−199.
(15) Kim, K. Y. *Nanomed.: Nanotechnol., Biol., Med.* **2007**, *3*, 103−110.
(16) Goodman, T. T.; Olive, P. L.; Pun, S. H. *Int. J. Nanomed.* **2007**, *2*, 265−274.
(17) Dreher, M. R.; Liu, W. G.; Michelich, C. R.; Dewhirst, M. W.; Yuan, F.; Chilkoti, A. *J. Natl. Cancer Inst.* **2006**, *98*, 335−344.
(18) Nagano, S.; Perentes, J. Y.; Jain, R. K.; Boucher, Y. *Cancer Res.* **2008**, *68*, 3795−3802.
(19) Yuan, F.; Leunig, M.; Huang, S. K.; Berk, D. A.; Papahadjopoulos, D.; Jain, R. K. *Cancer Res.* **1994**, *54*, 3352−3356.

(20) Liu, Z.; Chen, K.; Davis, C.; Sherlock, S.; Cao, Q. Z.; Chen, X. Y.; Dai, H. J. *Cancer Res.* **2008**, *68*, 6652−6660.
(21) Ding, D.; Zhu, Z. S.; Li, R. T.; Li, X. L.; Wu, W.; Jiang, X. Q.; Liu, B. R. *ACS Nano* **2011**, *5*, 2520−2534.
(22) Nishiyama, N.; Yokoyama, M.; Aoyagi, T.; Okano, T.; Sakurai, Y.; Kataoka, K. *Langmuir* **1999**, *15*, 377−383.
(23) Chen, Y.; Ding, D.; Mao, Z. Q.; He, Y. F.; Hu, Y.; Wu, W.; Jiang, X. Q. *Biomacromolecules* **2008**, *9*, 2609−2614.
(24) Li, X. L.; Li, R. T.; Qian, X. P.; Ding, Y. T.; Tu, Y. X.; Guo, R.; Hu, Y.; Jiang, X. Q.; Guo, W. H.; Liu, B. R. *Eur. J. Pharm. Biopharm.* **2008**, *70*, 726−734.
(25) Prudêncio, M.; Rohovec, J.; Peters, J. A.; Tocheva, E.; Boulanger, M. J.; Murphy, M. E. P.; Hupkes, H. J.; Kosters, W.; Impagliazzo, A.; Ubbink, M. *Chem.—Eur. J.* **2004**, *10*, 3252−3260.
(26) Hu, Y.; Jiang, X. Q.; Ding, Y.; Chen, Q.; Yang, C. Z. *Adv. Mater.* **2004**, *16*, 933−937.
(27) Zhang, Y. W.; Wang, Z. X.; Wang, Y. S.; Zhao, H. X.; Wu, C. X. *Polymer* **2007**, *48*, 5639−5645.
(28) Tseng, C. L.; Wu, S. Y. H.; Wang, W. H.; Peng, C. L.; Lin, F. H.; Lin, C. C.; Young, T. H.; Shieh, M. J. *Biomaterials* **2008**, *29*, 3014−3022.
(29) Cabral, H.; Nishiyama, N.; Okazaki, S.; Koyama, H.; Kataoka, K. *J. Controlled Release* **2005**, *101*, 223−232.
(30) Diagaradjane, P.; Deorukhkar, A.; Gelovani, J. G.; Maru, D. M.; Krishnan, S. *ACS Nano* **2010**, *4*, 4131−4141.
(31) Zhang, L. Y.; Yang, M.; Wang, Q.; Li, Y.; Guo, R.; Jiang, X. Q.; Yang, C. Z.; Liu, B. R. *J. Controlled Release* **2007**, *119*, 153−162.
(32) Liu, Z.; Davis, W.; Cai, W.; He, L.; Chen, X. Y.; Dai, H. J. *Proc. Natl. Acad. Sci. U.S.A.* **2008**, *105*, 1410−1415.
(33) Gaumet, M.; Vargas, A.; Gurny, R.; Delie, F. *Eur. J. Pharm. Biopharm.* **2008**, *69*, 1−9.
(34) Li, S. D.; Huang, L. *Mol. Pharmaceutics* **2008**, *5*, 496−504.
(35) Tang, N.; Du, G. J.; Wang, N.; Liu, C. C.; Hang, H. Y.; Liang, W. *J. Natl. Cancer Inst.* **2007**, *99*, 1004−1015.
(36) Cheng, C.; Wei, H.; Zhu, J. L.; Chang, C.; Cheng, H.; Li, C.; Cheng, S. X.; Zhang, X. Z.; Zhuo, R. X. *Bioconjugate Chem.* **2008**, *19*, 1194−1201.
(37) Bai, S.; Wang, F.; Zhang, Z.; Li, S.; Zhang, J.; Zhang, Y. *J. Genet. Genomics* **2010**, *37*, 341−346.
(38) Zhu, Z. S.; Li, Y.; Li, X. L.; Li, R. T.; Jia, Z. J.; Liu, B. R.; Guo, W. H.; Wu, W.; Jiang, X.Q. *J. Controlled Release* **2010**, *142*, 438−446.
(39) Kurihara, N.; Kubota, T.; Hoshiya, Y.; Otani, Y.; Watanabe, M.; Kumai, K.; Kitajima, M. *J. Surg. Oncol.* **1996**, *61*, 138−142.
(40) Okino, H.; Maeyama, R.; Manabe, T.; Matsuda, T.; Tanaka, M. *Clin. Cancer Res.* **2003**, *9*, 5786−5793.